

CO OBSERVATIONS OF THE GALACTIC STAR-FORMING REGION W58

F. P. ISRAEL

Owens Valley Radio Observatory, California Institute of Technology, Pasadena; and
 Goddard Institute for Space Studies, New York

Received 1979 June 21; accepted 1979 September 13

ABSTRACT

Observations of ^{12}CO and ^{13}CO have been made in the direction of the strong galactic radio source W58, which contains the compact H II regions K3-50 and ON-3. An extended molecular cloud with dimensions of 55×40 pc is associated with the northern part of the H II region complex. The density of the molecular cloud increases from west to east; the molecular cloud is bounded on the east by a larger H I cloud. Present star-formation activity is taking place at the position of maximum molecular density, at what appears to be the interface of the H I cloud and the H II region complex. The velocity structure of the CO cloud and the compact H II regions are in agreement with the blister model. Radio continuum and H I line observations show indications of a shell structure in the southwest of W58. Present star formation in W58 may be caused by this expanding shell.

Subject headings: interstellar: molecules — nebulae: individual — radio sources: lines — stars: formation

I. INTRODUCTION

The strong galactic radio source W58 (Westerhout 1958) is an active region of star formation, probably representing the first stage of a massive OB association containing at least a dozen O stars (Israel 1976). A remarkable group of dense and compact H II regions is found at the position of peak radio emission. The compact H II regions G70.29+1.60 (K3-50) and G70.33+1.59 (ON-3) have been well studied at optical, infrared, and radio wavelengths.

The most compact and therefore youngest H II regions are concentrated toward one side of the complex; there is considerable extinction in the direction of some of them (Wynn-Williams *et al.* 1977; Thronson and Harper 1979), thus indicating the presence of neutral material with high column densities. On a much larger scale, the whole H II region complex is associated with an extended neutral hydrogen cloud (Bridle and Kesteven 1970). W58 was therefore considered to be a good candidate for mapping in the CO molecular line.

II. OBSERVATIONS

All observations described in this paper were made in 1976 March and April with the use of the Columbia University and the Texas Millimeter Wave Observatory telescopes.¹

a) New York Observations

First, ^{12}CO emission was observed with the Columbia University 1.2 m telescope in New York

¹The Millimeter Wave Observatory (MWO) at Fort Davis, Texas, is operated by the Electrical Engineering Research Laboratory, University of Texas at Austin, with support from the National Science Foundation and McDonald Observatory.

City. This telescope has a full beamwidth at half-power of $8'$ and a beam efficiency of 70% at the frequency of the $J = 1 \rightarrow 0$ transition of ^{12}CO (115 GHz). The receiver had a single-sideband noise temperature of 1500 K. The spectrometer consisted of a filterbank with a total bandwidth of 40 MHz and a spectral resolution of 1 MHz (corresponding to 2.6 km s^{-1} at 115 GHz). Since the observations were made by frequency-switching, the velocity range used was 52 km s^{-1} . The integration time per point was 3 minutes; several positions were observed more than once in order to check the system stability and the data quality.

The receiver was calibrated against a room-temperature blackbody by a chopper-wheel technique similar to that described by Davis and Vanden Bout (1973). An additional atmospheric correction was applied, taking into account the different scale heights of atmospheric water vapor and oxygen. The optical depth of water was derived from antenna dippings, and was usually between 0.1 and 0.3 at the zenith. The resulting $8'$ map was then used to determine which areas were of sufficient interest to warrant further mapping at higher resolution.

b) Texas Observations

The MWO 5 m telescope has a half-power beamwidth of $2.3'$ and a beam efficiency of 85% at 115 GHz. The receiver had a single-sideband noise temperature varying from 1500 to 2000 K. The filterbank had a total bandwidth of 10 MHz and a resolution of 250 kHz (0.65 km s^{-1} at 115 GHz). Again, all observations were made by frequency switching and the integration time per point was 5 minutes. Calibration and correction procedures were similar to the ones described above.

III. RESULTS AND ANALYSIS

a) *Distribution of CO in W58*

^{12}CO emission observed with $8'$ resolution integrated over all observed velocities is shown in Figure 1. The maximum roughly coincides with the peak radio emission (see Israel 1976) at $\alpha = 19^{\text{h}}57^{\text{m}}40^{\text{s}}$, $\delta = 33^{\circ}25'$.

Emission also extends to the north and south; the southern region coincides with extensive extinction features on Palomar Sky Survey prints. Although the eastern part of the map in Figure 1 was not fully sampled, considerable structure appears to be present in the southeast. Little CO emission is seen in the direction of the very extended, low surface brightness part of W58.

The main ^{12}CO complex is instead limited to the high surface brightness part of the radio source. Its size is $21' \times 15'$, corresponding to 55×40 pc at an assumed distance of 9 kpc. Almost all of the observed CO emission is contained in the velocity interval -19 to -30 km s^{-1} . Figure 2 shows the results of the observations with 2.3 resolution (Texas telescope), integrated over the full range of observed velocities. The CO complex in Figure 1 now is seen to consist of at least three components.

^{12}CO emission centered on $V_{\text{LSR}} = -23$ km s^{-1} is shown in Figure 2a. Black dots indicate H II regions (Israel 1976). Figure 2b shows ^{13}CO observations of the northern CO complex, Figure 2c ^{12}CO observations of the southern H II region group G69.92+1.52 (source G), centered on $V_{\text{LSR}} = -65$ km s^{-1} .

The western CO component is associated with the H II region G70.15+1.73 (S99) and has a size of 2.8×6.5 (corresponding to 7.5×17.0 pc). The central component has a size of about $2'$ (5 pc); in its direction only relatively diffuse H II emission is seen. The eastern CO component is the strongest; it has

an overall size of about 10 pc. From a comparison between the ^{12}CO and ^{13}CO maps it is clear that in the eastern component the density and temperature structures are different; this will be further discussed in §§ IIIb and IIIc.

It is of interest to note that the most compact and presumably youngest H II region G70.33+1.59 (ON-3 = C) coincides almost exactly with the ^{12}CO and ^{13}CO peaks, whereas the more evolved regions G70.29+1.60 (K3-50 = A), G70.30+1.60 (source B), G70.28+1.59 (NGC 6857 = D), and G70.31+1.66 (source E) are located further toward the edge.

Indeed, there appears to be a spatial sequence of H II regions, indicative of an evolutionary sequence. West of ON-3 the compact sources A (K3-50) and B are located at the edge of the density maximum, though well within the CO temperature maximum (cf. Fig. 2). Source D is farther from the density peak; it is at the edge of the temperature maximum, as are sources E and F.

At the same time source C (ON-3) is probably youngest: it has the highest density and possesses an OH maser. Source A is somewhat less dense, and appears to be emerging from its dust cocoon; it is therefore somewhat older as well. Source B has a lower electron density than source A, but higher than source D. It thus appears to be intermediate in age. Source D (NGC 6857) is optically visible, like sources B and F; these sources appear to be the most evolved and oldest.

The central CO component is not associated with a compact H II region; however, one should note that the overall CO distribution follows very closely the distribution of thermal radio emission (cf. Figs. 3 and 4 in Israel 1976). Indeed, at the NW tip of the central component, an enhancement in the thermal emission is found that probably corresponds to a well-evolved, extended H II region with a size of ~ 4 pc. At this position, the red PSS print shows a dark bay (Fig. 1

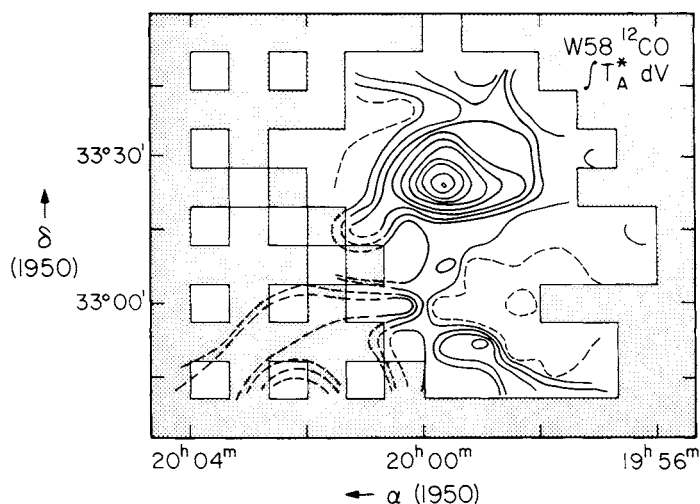


FIG. 1.— ^{12}CO map of W58 at $8'$ resolution (Columbia University telescope), integrated over a velocity range of 52 km s^{-1} . Thin lines indicate the area observed. Contour values are in steps of 2.6 K km s^{-1} . Zero contour and poorly observed contours are dashed.

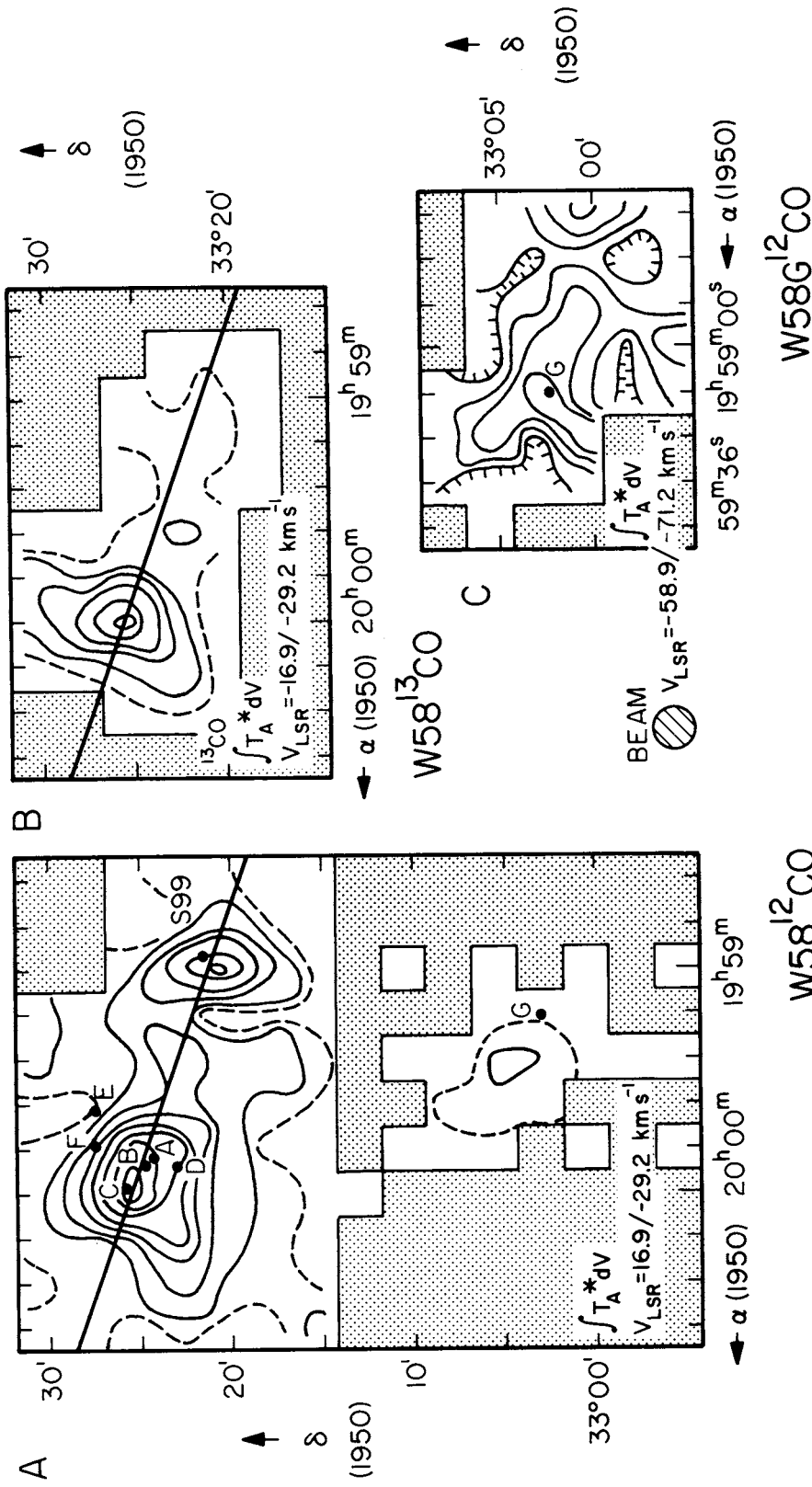


FIG. 2.— ^{12}CO and ^{13}CO maps of W58 at 2;3 resolution (MWO) integrated over a velocity range of 13 km s^{-1} . Thin lines indicate area observed. (a) ^{12}CO map. Contour values are in steps of 6.5 K km s^{-1} . Black dots indicate positions of H II regions mapped by Israel (1976), identified at the side of the map. (b) ^{13}CO map. Contour values are in steps of 3.25 K km s^{-1} ; zero contour is dashed. (c) ^{12}CO map of W58G. Contour values range from 1.63 to 6.5 K km s^{-1} . The position of source G is marked by a black dot.

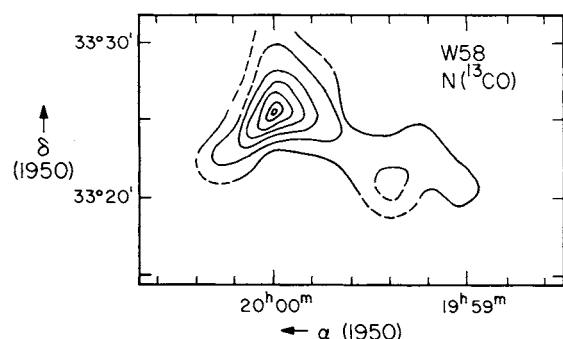


FIG. 3.— ^{13}CO column densities. Contour values range from 3×10^{15} to $27 \times 10^{15} \text{ cm}^{-2}$.

in Israel 1976). The eastern CO component is associated with the extended (2 pc) H II region S99.

b) Density Structure and Mass

From the observed ^{12}CO and ^{13}CO parameters, I calculated the ^{13}CO column densities under the usual LTE assumptions (see, e.g., Elmegreen and Elmegreen 1978). The resulting density distribution is shown in Figure 3.

Except in the eastern component, the column density is everywhere in the range $N(^{13}\text{CO}) = 1\text{--}6 \times 10^{15} \text{ cm}^{-2}$; the peak column density in the eastern component is $N(^{13}\text{CO}) = 3.5 \times 10^{16} \text{ cm}^{-2}$. In this component, the material seems to be distributed in a SE-NW ridge. I determined molecular hydrogen column densities using Dickman's (1978) relation $N(\text{H}_2) = (5 \pm 2.5) \times 10^5 N(^{13}\text{CO})$. For the eastern component I took the average within the $N(^{13}\text{CO}) = 5 \times 10^{15} \text{ cm}^{-2}$ contour; for the rest I took the average value $N(^{13}\text{CO}) = 3 \times 10^{15} \text{ cm}^{-2}$, and sizes from the ^{12}CO map (Fig. 2a). The line-of-sight depths were taken to be equal to the observed mean diameter in the ^{12}CO map. These assumptions lead to the molecular hydrogen space densities and masses in Table 1. In column (7) the mean density is given as well as a value representative of the dense cores.

It should be mentioned here that the density and mass values listed in Table 1 are probably lower limits, since the three components are hardly resolved because of the linear beamsize of 7 pc at a distance of 9 kpc. Also, at least in the core of the eastern component, ^{13}CO may be underabundant (see Wootten *et al.* 1978). Indeed, use of Dickman's (1978) relationship of column density $N(^{13}\text{CO})$ to visual extinction

yields maximum values for the extinction of only $A_V \approx 10$ mag, appreciably less than $A_V \approx 100$ mag derived for ON-3 from far-infrared measurements (see § IIIc). The latter value can be recovered, however, if ^{13}CO is underabundant by an order of magnitude as discussed in detail by Rowan-Robinson (1979). A comparison with infrared observations of compact H II regions associated with the eastern component nevertheless indicates that the overall values in Table 1 are generally correct.

One-millimeter observations by Wynn-Williams *et al.* (1977) show considerable amounts of dust near both K3-50 and ON-3. They estimate space densities of $n(\text{H}_2) = 1.5 \times 10^4 \text{ cm}^{-3}$ and column densities of $N(\text{H}_2) = 1 \times 10^{23} \text{ cm}^{-2}$ as compared to $n(\text{H}_2) = 2 \times 10^3$ to $6 \times 10^4 \text{ cm}^{-3}$ and $N(\text{H}_2) = 7 \times 10^{22} \text{ cm}^{-2}$ derived from the present CO observations. Similar good agreement is found with the far-infrared results obtained by Thronson and Harper (1979) from which $N(\text{H}_2) = 2\text{--}6 \times 10^{22} \text{ cm}^{-2}$ can be derived.

c) Velocity Structure

The velocity structure of the W58 CO complex is shown in Figures 4 and 5. Figure 4 presents the ^{12}CO intensity at different velocities, averaged over two velocity channels. The velocity structure of the strong eastern CO component is remarkable. At velocities $V_{\text{LSR}} = -23.7 \text{ km s}^{-1}$ the cloud is elongated in a SE-NW direction, while a broader NE-SW elongation is seen at $V_{\text{LSR}} = -25.0 \text{ km s}^{-1}$. This aspect is further illustrated in Figure 5a. Figures 5a and 5b show the velocity structure of ^{12}CO and ^{13}CO , respectively, as a function of position along the lines marked in Figures 2a and 2b. In Figure 5a the three major components stand out clearly. They have the same velocity within 0.3 km s^{-1} . The position shift at more negative velocities ($V_{\text{LSR}} = -23.7 \text{ km s}^{-1}$) is very clear; at the same time the emission is broader. The velocity map of ^{13}CO presents a different aspect. The eastern component is easily visible, but the other two are rather weak. There is only a faint trace of the negative velocity wing in the form of a weak extension to the west at $V_{\text{LSR}} = -24.3 \text{ km s}^{-1}$.

An interesting comparison can be made with the velocities of the strongest H II regions in the northern part of W58. High-resolution H109 α recombination-line observations have been made with the Westerbork Synthesis Radio Telescope by van Gorkom *et al.* (1979). The velocities for the sources A, B, C, and D range from -16 km s^{-1} to -31 km s^{-1} . Sources A

TABLE 1
RESULTS OF W58 CO OBSERVATIONS

Component (1)	Peak T_A^* (^{12}CO) (K) (2)	Peak T_A^* (^{13}CO) (K) (3)	ΔV (^{13}CO) (km s^{-1}) (4)	Mean Size (pc) (5)	Peak N (^{13}CO) (cm^{-2}) (6)	n (H_2) (cm^{-3}) (7)	Mass (M_\odot) (8)
West.....	7.6	1.2	2.5	11	3.1×10^{15}	100–350	2.4×10^3
Central.....	4.9	1.8	3.0	5	6.1×10^{15}	200–1000	1.2×10^3
East.....	10.0	4.4	5.0	10	2.9×10^{16}	$2 \times 10^3\text{--}6 \times 10^4$	1.1×10^5

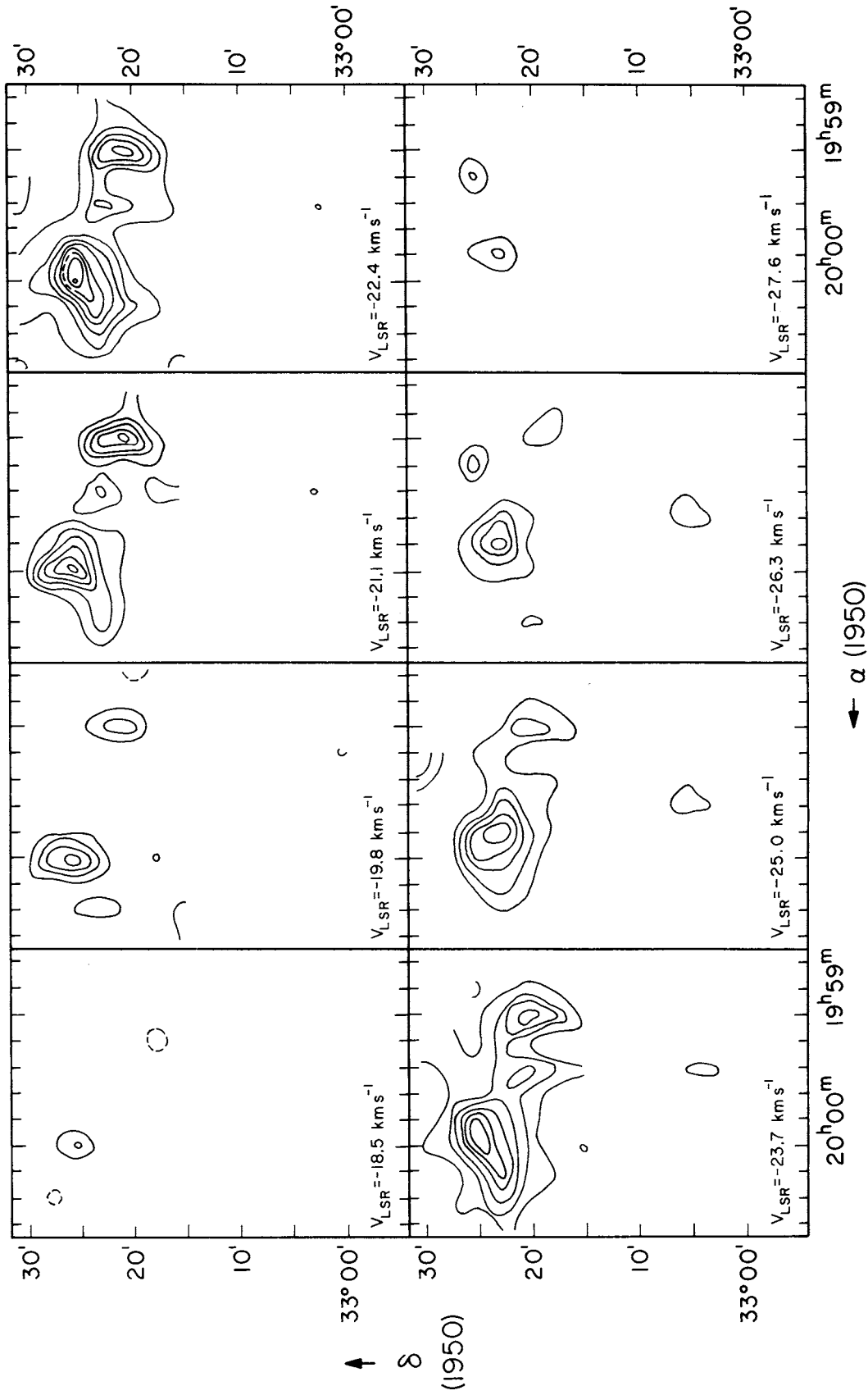


FIG. 4.— ^{12}CO maps at different velocities integrated over two channels. Contour values are in steps of 1.63 K km s^{-1} . Negative contours are dashed, zero contour is omitted.

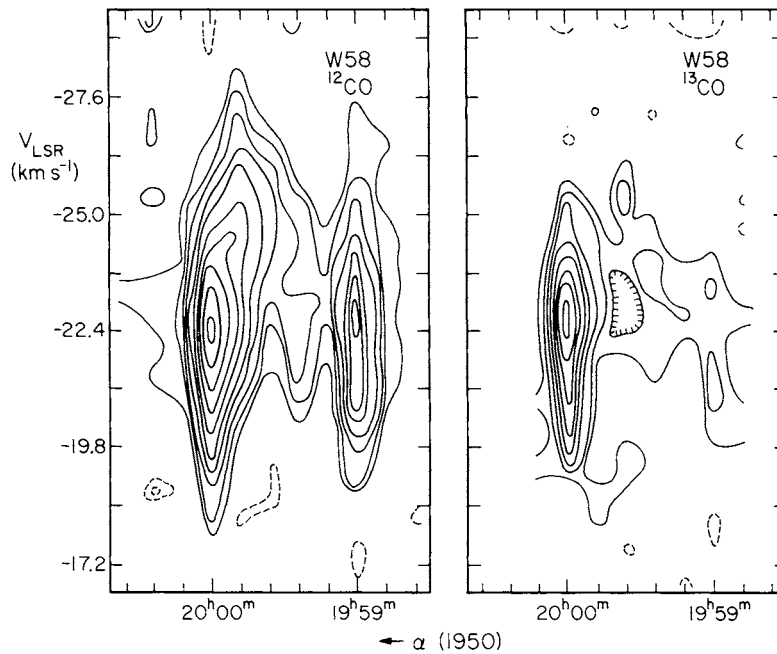


FIG. 5.— ^{12}CO and ^{13}CO velocity distribution along the lines marked in Figs. 2a and 2b. Contour values are in steps of 0.65 K km s^{-1} for ^{12}CO and 0.33 K km s^{-1} for ^{13}CO . Velocities toward the observer are at the top.

(K3-50) and D (NGC 6857) have the most negative velocities, and appear to be associated with the high-temperature CO of relatively low density. The velocity of K3-50 is considerably more negative than that of the bulk of the CO cloud in the same direction, the velocity of NGC 6857 moderately so. This suggests that in these two sources the ionized gas streams away from the molecular cloud with velocities of $5\text{--}10 \text{ km s}^{-1}$, and that they are located at the near side of the cloud, in good agreement with the blister model (Israel 1978). The blister model also appears applicable to sources B and C (ON-3). In this case source B should be somewhat beyond the western edge of the molecular cloud, and should have mainly transverse velocities. Source C has a radial velocity 6 km s^{-1} less negative than the molecular cloud, and therefore should be located at the far side of the cloud (see also van Gorkom *et al.* 1979). The extinction properties of these H II regions strongly support this interpretation: source A is partly obscured by a dense dark cloud in its immediate vicinity (Israel 1976, and references therein; Wynn-Williams *et al.* 1977), while source C (ON-3) has a very high extinction ($A_V \approx 100 \text{ mag}$; Wynn-Williams *et al.* 1977).

The H II region group G69.92 + 1.52 (source G) has a radial velocity of -65 km s^{-1} (Downes and Wilson 1974) that is different by more than 40 km s^{-1} from the velocity of the northern components. Yet it is unlikely that it is at a farther distance than these, since its kinematical distance would place it at the other side of the Perseus Arm. Its optical visibility seems to rule out this possibility. Another indication that source G is physically connected to the W58 complex is furnished by the CO maps in Figure 2.

CO emission is visible near source G at both velocities, although more strongly at the velocity $V_{\text{LSR}} = -65 \text{ km s}^{-1}$.

A velocity dispersion of 40 km s^{-1} is, however, quite large for H II region groups. A possible explanation is given in the next section.

d) Comparison with Neutral Hydrogen

A comparison of Figure 4c from Bridle and Kesteven (1970) with Figures 5a and 5b in this paper clearly shows that the CO cloud has a velocity about 6 km s^{-1} less negative than the H I cloud complex at the same position. In fact, the H I cloud has the same velocity only at more northern declinations, at about $\alpha = 20^{\text{h}}01^{\text{m}}\text{--}20^{\text{h}}02^{\text{m}}$.

More recently, P. L. Read (private communication) has obtained H I data with the Cambridge Half Mile Synthesis Telescope at roughly 3 times better resolution. His results show a remarkable correlation between the H I and CO distributions. The western CO component (S99) lies at the western edge of the H I peak. The peak H I emission is distributed in a long ridge, elongated in the SE-NW direction. The eastern CO component seems to follow this ridge, even to the extent that the upper curve to the SW follows a protuberance in the H I distribution. Moreover, the line connecting the three CO maxima almost bisects the H I ridge at right angles. The unresolved northeastern edge of the main CO component appears to be the interface between the CO cloud/H II region complex and the H I cloud. In the $8'$ (New York) map (Fig. 1), the weak CO extension to the SW still follows the H I ridge; the poorly sampled CO emission in the

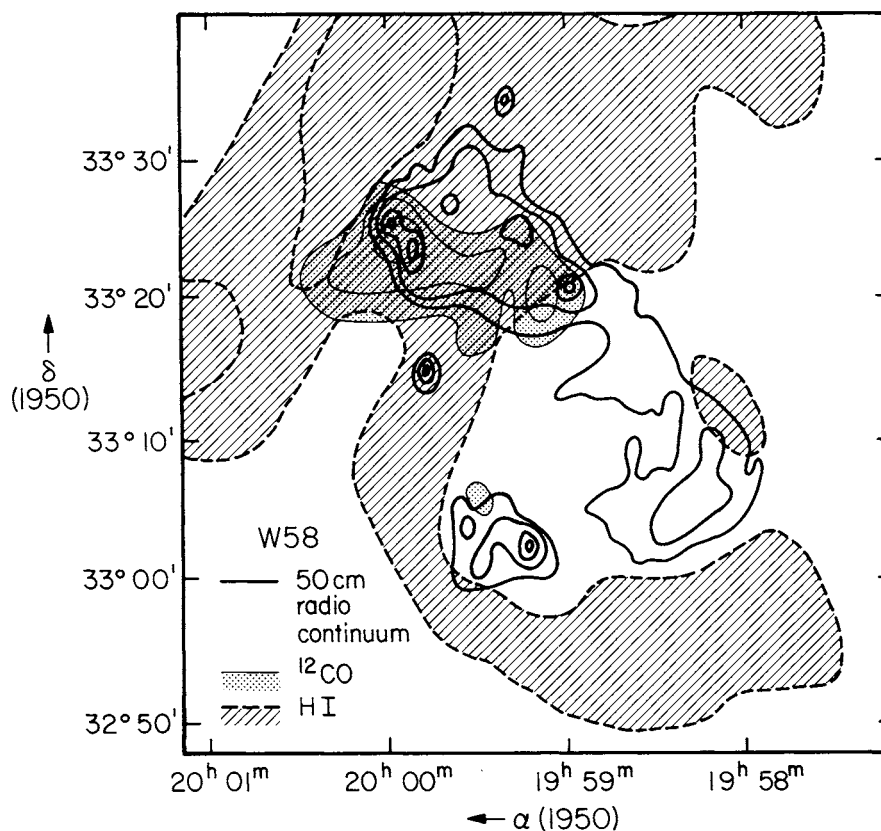


FIG. 6.—Very schematic representation of W58 observations in radio continuum (Israel 1976), ^{12}CO (this paper) and H I (Read, private communication).

SE corner of the map occupies a minimum in the H I distribution, and the CO ridge in the SW corner of the map again lies at the (eastern) edge and follows an H I feature extending from K3-50 through source G.

A comparison of the 0.6 GHz radio continuum map (Israel 1976) and Read's H I map shows an intriguing state of affairs; see, for instance, Figure 6.

The southwest radio component has the shape of an incomplete shell with outer diameter $24'$ (65 pc), and a thickness of about $2.5'$ (7 pc). If one completes the shell, both source G and S99 are placed on it. At the same position, Read's H I map also shows a shell structure, with an outer diameter of roughly $28'$ (75 pc) and a thickness of $5.5'$ (14 pc). Little can be said about the kinematics of the H I since the velocity coverage of the Cambridge H I map is very limited, while Bridle and Kesteven's (1970) map has insufficient resolution. With an expansion velocity of order $50\text{--}100\text{ km s}^{-1}$ the problem of the discrepant velocity of source G is solved.

IV. CONCLUSION: STAR FORMATION IN W58

The observational results presented in the preceding section can be used to obtain information on the process of star formation in W58.

Going from WSW to ENE, there appears to be an

evolutionary sequence of H II regions in the sense that the most evolved and presumably oldest H II regions are in the west, while the youngest are in the east (§ IIa). At the same time there is a density increase in the molecular cloud from west to east. The youngest H II regions are associated with the densest part of the CO cloud, and appear to be located at the edge of the density maximum (§ IIIb). The CO density maximum takes the shape of a relatively narrow ridge directly adjacent to the broader and more extended ridge of strong H I emission, but is at a slightly different velocity (§§ IIIb and IIIc). This strongly suggests that the main CO maximum is the actual interface of the H I cloud and the extended H II region complex. The morphology and velocity structure suggest that the H I/CO/H II complex is seen more or less edge-on.

The present site of star formation, as marked by the ultra-compact H II region/OH maser source ON-3 and the emerging compact H II region K3-50, coincides with the CO density peak at the H I/H II interface. At the other end of the ENE-WSW axis of the CO complex we find S99. Because of its relatively low rms electron density it probably is an older, well-evolved region. The lack of high-density CO points in the same direction. Nevertheless, it is unlikely to be much older than $5\text{--}10 \times 10^5$ years. At a distance of 9 kpc, the angular distance of $13.5'$ between ON-3 and

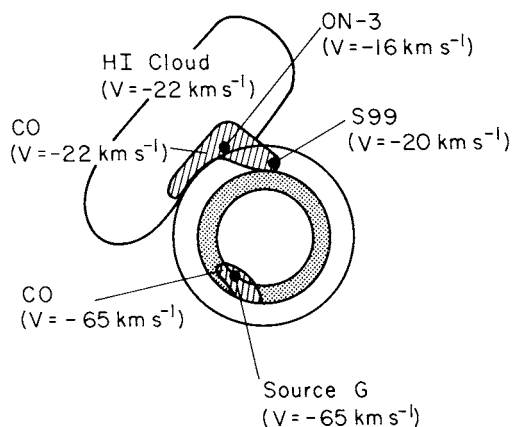


FIG. 7.—Schematic representation of W58. Blank regions indicate H I emission, dashed regions CO emission, and black dots H II regions. For further explanation, see text.

S₉₉ translates into a linear projected distance of 35 pc. Given these values, it is improbable that the Elmegreen and Lada (1977) model applies to this source, since it would imply a propagation velocity for the star-forming process of at least 35–70 km s⁻¹.

It is also unlikely that a galactic density wave triggered star formation in W58, since the complex appears to be located in interarm space (cf. the H I absorption data by Bridle and Kesteven 1970; and by Thompson, Colvin, and Hughes 1969).

The most likely cause of star formation, albeit an uncertain one with the present data, seems to be interaction of the large H I ridge with the radio continuum/H I shell mentioned in § III d. Unfortunately, while the shell is clearly delineated in the west, the more interesting eastern side is difficult to trace. The H I tongue that descends from K3-50 through source G is probably only a bright part of the near side of the shell—thus the shell extends farther to the east and is in contact with the ridge. This situation is illustrated in Figure 7. However, the possibility that the H I tongue actually marks the eastern boundary of the shell cannot entirely be ruled out. In that case, shell and star formation would be unrelated.

What is the nature of the shell? The large size of the radio continuum shell makes it unlikely that it is a supernova remnant. Its surface brightness is $\Sigma_{0.6\text{GHz}} = 2.2\text{--}3.1 \times 10^{-21} \text{ W m}^{-2} \text{ sr}^{-1} \text{ Hz}^{-1}$, whereas one would expect $\Sigma_{0.6\text{GHz}} = 1.9\text{--}4.3 \times 10^{-19} \text{ W m}^{-2} \text{ sr}^{-1} \text{ Hz}^{-1}$ on the basis of any reasonable Σ -d relationship (see, e.g., Ilovaisky and Lequeux 1972; Caswell and Lerche 1979; Milne 1979). This difference

of two orders of magnitude seems to rule out the possibility of a supernova remnant, even if one allows for the fact that the shell is not expanding into a low-density environment.

A more attractive possibility is that the H I/H II shell is created by strong stellar winds originating from OB stars formed at an earlier epoch. If all the observed radio continuum emission in the south of W58 is due to thermal bremsstrahlung, at least two O5 stars, or more likely a small cluster of OB stars, must be present in order to explain the observed radio intensity.

Moreover, with a linear outer diameter of 75 pc and a total H I mass of $1.2 \times 10^6 M_{\odot}$ [assuming $n(\text{H I}) = 100 \text{ cm}^{-3}$] the shell in W58 would be comparable to the H I shells discussed by Heiles (1976, 1979). Application of the interstellar bubble model by Castor, McCray, and Weaver (1975) to the observations yields an age of 10⁷ years for the shell. For a $V_{\text{shell}} = 50 \text{ km s}^{-1}$ the average energy loss rate of the stars is $dE/dt = 9.2 \times 10^{37} \text{ ergs s}^{-1}$, or $dE/dt = 37 \times 10^{-6} M_{\odot} \text{ yr}^{-1} \times (2000 \text{ km s}^{-1})^2$ in the units adopted by these authors.

I suggest the following scenario: About 10⁷ years ago star formation started in the W58 region. Stellar winds streaming away from the newly formed stars caused an expanding bubble to form. The inside of the resulting shell is ionized by the same stars. In more recent times, the expanding shell has interacted with nearby neutral clouds, thereby triggering a new epoch of star formation in these clouds. Source G and S99 would be the first to form in this secondary wave of star formation. At present, the shell is colliding with a large H I cloud to the northeast of W58, and current star formation is taking place at the interface.

Thus most of the W58 complex is beyond the star-forming stage. Only in the northeast is enough mass present to sustain star formation in the future.

I am much indebted to Pat Thaddeus for his encouragement and hospitality at the Goddard Institute for Space Studies. The observations were obtained thanks to the helpful efforts of Leo Blitz, George Tomasevich, Richard Cohen, and Hong-ih Cong; I am also grateful to Peter Read and Jacqueline van Gorkom, who sent me their results prior to publication. Anneila Sargent and Alan Moffet kindly commented on a draft of this paper. Finally, I acknowledge support by the Sterrewacht at Leiden, and NSF grant AST 077-00247.

REFERENCES

- Bridle, A. H., and Kesteven, M. J. L. 1970, *A.J.*, **75**, 902.
 Castor, J., McCray, R., and Weaver, R. 1975, *Ap. J. (Letters)*, **200**, L107.
 Caswell, J. L., and Lerche, I. 1979, *Australian J. Phys.*, **32**, 79.
 Davis, J. H., and Vanden Bout, P. 1973, *Ap. J.*, **15**, 43.
 Dickman, R. L. 1978, *Ap. J. Suppl.*, **37**, 407.
 Downes, D., and Wilson, T. L. 1974, *Astr. Ap.*, **34**, 133.
 Elmegreen, D. M., and Elmegreen, B. G. 1978, *Ap. J.*, **219**, 105.
 Elmegreen, B. G., and Lada, C. J. 1977, *Ap. J.*, **214**, 725.
 Heiles, C. 1976, *Ap. J. (Letters)*, **208**, L137.
 ———. 1979, *Ap. J.*, **229**, 533.
 Ilovaisky, S. A., and Lequeux, J. 1972, *Astr. Ap.*, **18**, 169.
 Israel, F. P. 1976, *Astr. Ap.*, **48**, 193.
 ———. 1978, *Astr. Ap.*, **70**, 769.
 Milne, D. K. 1979, *Australian J. Phys.*, **32**, 83.
 Rowan-Robinson, M. 1979, preprint.

- Thompson, A. R., Colvin, R. S., and Hughes, M. P. 1969, *Ap. J.*, **158**, 939.
- Thronson, H. A., and Harper, D. A. 1979, *Ap. J.*, **230**, 133.
- van Gorkom, J. H., Shaver, P. A., Blair, G. N., Matthews, H. E., and Pottasch, S. R. 1979, *Astr. Ap.*, in press.
- Westerhout, G. 1958, *Bull. Astr. Inst. Netherlands*, **14**, 215.
- Wooten, A., Evans, N. J., Snell, R. L., and Vanden Bout, P. A. 1978, *Ap. J. (Letters)*, **225**, L143.
- Wynn-Williams, C. G., Becklin, E. E., Matthews, K., Neugebauer, G., and Werner, M. W. 1977, *Ap. J.*, **179**, 255.

FRANK P. ISRAEL: Owens Valley Radio Observatory, California Institute of Technology, 102-24, Pasadena, CA 91125